

# Electron paramagnetic resonance oxygen imaging of a rabbit tumor using localized spin probe delivery

Boris Epel

Department of Radiation and Cellular Oncology, The University of Chicago, MC 1105, Chicago, Illinois 60637

Chad R. Haney

Department of Radiology, The University of Chicago, MC 2026, Chicago, Illinois 60637

Danielle Hleihel

Department of Radiation and Cellular Oncology, The University of Chicago, MC 1105, Chicago, Illinois 60637

Craig Wardrip

Department of Surgery, Animal Resource Center, The University of Chicago, MC 1030, Chicago, Illinois 60637

Eugene D. Barth and Howard J. Halpern<sup>a)</sup>

Department of Radiation and Cellular Oncology, The University of Chicago, MC 1105, Chicago, Illinois 60637

(Received 19 January 2010; revised 7 April 2010; accepted for publication 9 April 2010; published 13 May 2010)

**Purpose:** Application of *in vivo* electron paramagnetic resonance (EPR) oxygen imaging (EPROI) to tumors larger than those of mice requires development of both instrumental and medical aspects of imaging.

**Methods:** 250 MHz EPR oxygen imaging was performed using a loop-gap resonator with a volume exceeding 100 cm<sup>3</sup>. The paramagnetic spin probe was injected directly into the femoral artery feeding the rabbit leg/tumor.

**Results:** The authors present continuous wave and electron spin echo EPR oxygen images of a large size (4 cm) VX-2 tumor located on the leg of a New Zealand white rabbit.

**Conclusions:** This study demonstrates the feasibility of continuous wave and electron spin echo oxygen imaging modalities for investigation of volumes of tumor and normal tissue relevant to large animals. The injection of the spin probe directly into the artery feeding a rabbit leg will allow one to reduce, by over one order of magnitude, the amount of spin probe used as compared to whole animal IV injection. © 2010 American Association of Physicists in Medicine.

[DOI: [10.1118/1.3425787](https://doi.org/10.1118/1.3425787)]

Key words: electron paramagnetic resonance, electron spin echo, oxygen imaging, oxygen, hypoxia

## I. INTRODUCTION

Electron paramagnetic resonance (EPR) imaging<sup>1-4</sup> is a versatile technique that has been applied to a number of biological problems<sup>5</sup> and promises eventual medical application.<sup>6,7</sup> Due to the very low natural concentration of paramagnetic species in living tissues, exogenous spin probes, with stable unpaired electrons, need to be injected into animal subjects. Specific spin probes report various characteristics of the fluids in which they distribute through their EPR spectra. Of special value is the sensitivity of EPR spectral linewidths to oxygen partial pressure (pO<sub>2</sub>) in tissues.<sup>8</sup> Although other imaging techniques exist to image hypoxia<sup>9-12</sup> (see also Ref. 13 for a review), none of these techniques promise the spatial resolution, the quantification of pO<sub>2</sub>, and the consequent reproducibility of EPR oxygen images (EPROIs).<sup>14</sup> These oxygen images in point by point comparisons have been shown to quantitatively and spatially agree with *in situ* measurements employing an Oxylite™ fluorescence quenching

probe.<sup>15</sup> Using EPROI we have previously shown that oxygenation increases after treatment with a radiation mediated gene therapy in prostate cancer xenografts.<sup>16</sup> In murine fibrosarcomas it has been shown that EPR image based tumor hypoxic fractions sharpen the predictability of tumor cure when compared to dose alone.<sup>17</sup> These promising studies demonstrate the importance of oxygenation images in predicting tumor cure and indicate that determining spatial distributions of tumor oxygenation will enhance the effectiveness of localized cancer therapy, particularly intensity-modulated radiotherapy.<sup>18</sup> The majority of previous studies were performed on mice and rats. Thus, it is crucial to investigate the potential for scaling up EPROI to larger animals.

In general, larger animals require larger amounts of spin probe but, as shown below, the method of injection plays an important role in the quantity of probe needed. The most common spin probe used for oxygenation images in animals presently is the triarylmethyl radical OX063, referred also as

trityl.<sup>8,19</sup> This spin probe is administered systemically in mice via tail vein. A short time after the spin probe is infused, it distributes into extracellular volume of tissues of the entire animal giving rise to an EPR signal.<sup>20</sup> Renal excretion effectively removes the spin probe from the blood and deposits it into the bladder. After a single bolus spin probe infusion, there is a rapid decrease in the spin probe concentration in the animal body with a tissue half-life less than 5 min and tumor half-life of 30 min.<sup>14,19</sup> This alters the distribution of spin probe during the acquisition of image projections and affects image quality. This effect can be minimized using constant infusion of spin probe for the duration of the image after initial bolus as demonstrated in this work. The rate of this infusion varies from animal to animal due to weight, renal function, and tumor burden. The typical infusion rate in mice is about the amount of the initial bolus dose infused over 1 h.

While an infusion into rodent's tail vein eventually delivers spin probe to a tumor, spin probe is wasted in first pass kinetics and distribution over the entire animal body. Scaling of this probe administration method up to larger animals is not cost-effective. Moreover, for larger animals and human size subjects, this method presents an unnecessary trityl injection mass that should be avoided for localized images. Therefore, we developed a more localized delivery method.

Another aspect of larger animal imaging is the reduction in instrument's sensitivity associated with the increase in resonator's volume and decrease in resonator's efficiency. In our laboratory we employ two EPR oxygen imaging methodologies: Continuous wave (CW)<sup>3,4</sup> spectral-spatial imaging and electron spin echo (ESE).<sup>33</sup> Most of the previous results are obtained using resonators with volumes below 20 cm<sup>3</sup>. Therefore, the issue of scaling up EPR imaging technology to larger objects requires a thorough investigation. The images in a 50 mm i.d. loop-gap resonator (~100 cm<sup>3</sup>) obtained using our CW methodology have indicated good oxygen resolution in a phantom as large as the tumor-bearing rabbit leg.<sup>21</sup>

In this work, we examine the localized delivery of spin probe to the large tumor located on the leg of a rabbit. The oxygen and spin probe concentration in the tumor are monitored using CW and ESE imaging methodologies.

## II. MATERIALS AND METHODS

### II.A. Spin probe

The spin probe used for the EPR imaging was a OX063 radical methyl-tris[8-carboxy-2,2,6,6-tetrakis[2-hydroxyethyl]benzo[1,2-d:4,5-d'] bis[1,3] dithiol-4-yl]-trisodium salt, molecular weight=1427 (GE Healthcare, Little Chalfont, Buckinghamshire, U.K.). 70.0 mM OX063 solution was prepared in distilled water and then passed through a 5  $\mu$ m filter to remove particles large enough to occlude a capillary.

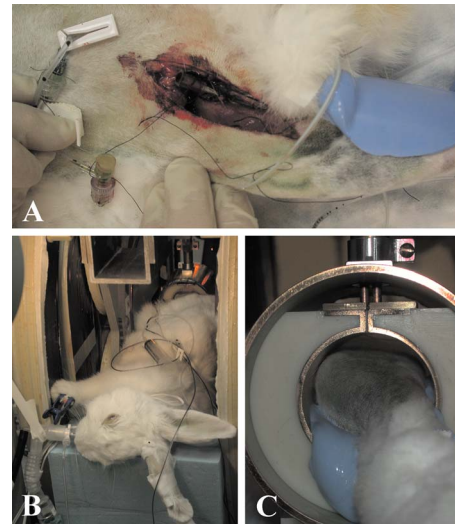


FIG. 1. (a) Cannulation of femoral artery feeding the leg tumor. (b) Rabbit in the magnet under gas anesthesia. (c) Tumor-bearing leg in loop-gap resonator.

### II.B. Animals and tumor

3 kg New Zealand white rabbits were supplied by Covance (USA). They were received at 11–13 weeks of age, were housed individually in climate-controlled, circadian rhythm-adjusted rooms, and were allowed food and water *ad libitum*. The culture of syngeneic VX-2 rabbit carcinoma was obtained as a kind gift from the Tumor Repository of the NCI Developmental Therapeutics Program, Division of Cancer Treatment and Diagnosis (Frederick, MD). The animal studied in this work was intramuscularly inoculated by a 14 Ga needle of 0.5 ml of coarsely minced tumor fragments. A roughly ovoid tumor grew to 41 mm maximum linear dimension in 4 weeks. All animal procedures were performed under Institutional Animal Care and Use Committee approved protocols.

### II.C. Direct cannulation of the artery feeding the immediate tumor environment

Prior to imaging, a patent, nonoccluding 27 Ga arterial catheter was installed in the femoral artery feeding the tumor-bearing leg of the rabbit. An incision was made in the mid thigh of the animal [see Fig. 1(a)]. Using blunt dissection, the femoral artery was isolated and the catheter was placed being careful that its diameter did not occlude the artery. A 10 ml syringe loaded with a 70 mM solution of OX063 was attached to the cannula, allowing direct intra-arterial infusion of spin probe into the tumor during imaging.

### II.D. Animal preparation for imaging

Throughout the preparation, transport, and EPR imaging, the animal breathed medical grade air containing ~1.5% isoflurane. Blood oxygen saturation, breathing rate, and rectal temperature were monitored throughout the preparation and imaging. The animal's body temperature was maintained by a combination of warm water pads and radiant heat. Fig-

ure 1(b) shows the intubated animal, while the tumor-bearing leg is installed in the resonator. The leg bearing the tumor is shown in Fig. 1(c).

### II.E. EPR resonator and animal layout

For EPR imaging, we used a single loop single gap resonator [see Fig. 1(c)]. The inductor/sample holder had an inner diameter of 50 mm, a length of 57.4 mm, and a volume of 112 ml. The resonator was fabricated from ABS plastic and electroplated with 12.5  $\mu\text{m}$  copper covered with 2  $\mu\text{m}$  gold. The similarly plated RF shield of the resonator was 9.1 cm in diameter and 7.6 cm long with no end caps. A layer of S00600 insulating varnish (Sherwin-Williams Co., Sprayon Products Group, Solon, OH) covered the inner surface of the shield of the resonator to prevent an electrical path from the resonator to the shield through the animal body. Both CW and ESE measurements were performed in the same resonator. The resonator was critically coupled at a frequency of 239.3 MHz with a loaded  $Q$  of 11.7. The rabbit's body was positioned along the axis of the resonator. Its tumor-bearing leg was centered in the resonator and immobilized using vinyl polysiloxane dental impression material (GC America, Inc., Alsip, IL) hardened with regular type Examix NDS hardener.<sup>22</sup> This material is relatively soft but retains its shape and is a major component in tumor/leg registration of multimodal images.

### II.F. Animal imaging

Prior to CW imaging, OX063 was injected through the intra-arterial catheter. A volume of 5 ml of the 70 mM solution (a total of 0.5 g) of OX063 was used for the initial bolus, followed by continuous infusion at the rate of 5 ml/h (0.5 g/h). For a 3 kg rabbit, this corresponds to 170 mg/kg body-weight (b.w.) for the first injection and 170 mg/kg b.w./h continuous infusion. Continuous infusion was maintained during both CW and ESE imaging. The duration of CW image acquisition was 48 min, while the duration of ESE acquisition was 13 min.

### II.G. Continuous wave imaging

The 250 MHz CW imager used in the study is described elsewhere.<sup>2,23</sup> 12 dBm of microwave power was used for the imaging, which corresponds to  $B_1$  of 1.2  $\mu\text{T}$ , required for oxygen measurements.<sup>14</sup> We used an overmodulation protocol with 5 kHz magnetic field modulation of 18  $\mu\text{T}$  peak-to-peak amplitude. For a 4D spectral-spatial image, we acquired projections at 14 spectral angles for each of 66 spatial directions, a total of 924. The spatial directions were selected using an equal solid angle algorithm.<sup>24</sup> The spatial and spectral fields of view were 11 cm and 0.1 mT, respectively. Projections were filtered with a 3D Ram-Lak filter with a cutoff at 0.5 times the Nyquist frequency and four times linearly interpolated.<sup>24,25</sup> The resulting 4D image obtained using filtered backprojection contained 64 point spectrum for each of 64<sup>3</sup> 3D spatial points. The fitting algorithm for overmodulated line shapes of Mailer *et al.*<sup>26</sup> was used to extract

the spin packet line width from the spectral dimension of each spatial voxel of the image. All data processing was performed using in-house MATLAB (The MathWorks, Inc., Natick, MA) programs.

### II.H. Pulse EPR imaging

The general design of the 250 MHz pulse imager used in this study is described elsewhere;<sup>27</sup> the new transmit/receive switch, used here, is described elsewhere.<sup>28</sup> 500 W of RF power was used to generate an ESE sequence with  $\pi/2$  and  $\pi$  pulses with durations of 60 and 120 ns, respectively. The duration of the pulses was dictated by the maximum available RF power. The influence of the RF pulses frequency profile on image intensity was compensated as described in Ref. 27. We acquired five images with delays between the pulse pairs logarithmically spaced in the range from 650 ns and 2  $\mu\text{s}$ . For each image, we acquired 164 projections and 42 interleaved baselines for artifact suppression. The maximum gradient amplitude was 0.5 G/cm; an equal solid angle scheme<sup>24</sup> was used for gradient directional spacing. The ESE data acquisition and processing methods are discussed in detail elsewhere.<sup>27</sup>

### II.I. Concentration calibration

The concentration of the spin probe in the rabbit was determined by comparison of the extrapolated to time 0 signal intensity derived from the rabbit image with that of an image of a 1 mM OX063 deoxygenated solution. The CW and ESE images of 1 mM OX063 solution were recorded in the same resonator using the same acquisition parameters. The loaded  $Q$  of resonator was brought down to 11.7 by inserting a tube with appropriate volume of 5M NaCl solution.

### II.J. MRI imaging and image registration

For the identification of the tumor region, we have obtained MRI image of the rabbit leg. After the EPR image was obtained, the rabbit was sacrificed using first high dose anesthesia and then 200 mg/kg injection of pentobarbital. The rabbit leg was then carefully separated from the animal body, retaining its immobilizing cast and preserved in formalin for 12 h. Our experience with living and postmortem MRI images indicates a substantial retention of  $T_2$  MRI contrast with this procedure, enough so that tumor definition is not compromised. The tumor-bearing leg was imaged using a 9.4 T, 30 cm diameter bore Bruker MRI scanner equipped with self-shielded imaging gradients with a Bruker linear, volume, 72 mm birdcage coil. For image registration and anatomical guidance, the multislice, rapid acquisition with relaxation enhancement (RARE) spin echo sequence (TR=4000 ms, effective TE=28 ms, FOV=8.0 cm, matrix size=256 $\times$ 256, slice thickness=1.0 mm, NEX=1, and RARE factor=4) was used. Images were acquired in planes roughly orthogonal to the long axis of the leg, approximating a transaxial plane (the XZ plane in Fig. 3).

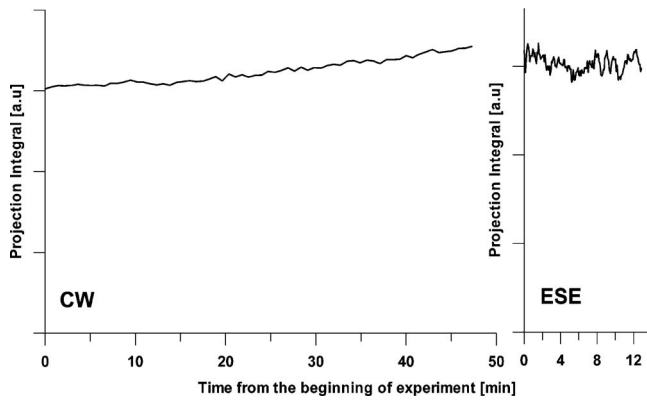


FIG. 2. The integrated intensity of CW and ESE projections as a function of the time over the image acquisition. For CW acquisition, the integrals for projections with the lowest gradient are presented. For ESE the integrals for projections recorded with  $\tau=860$  ns are presented.

The tumor outline was manually contoured in an MRI that was registered with the EPROI and then transferred to the EPR image. EPR and MRI images were manually registered using the Arbutus toolbox for MATLAB developed in our laboratory. The spatial correspondence between images was obtained by means of registering fiducials (i.d. of 1.2 mm) inserted into holes in the vinyl polysiloxane cast. For MRI we used fiducials of identical diameter filled with 1 mM solution of  $\text{CuSO}_4$ , while for EPR imaging a solution of deuterated Finland trityl with 35 mG line width was used. The fiducial EPR image was taken prior to oxygen image. After that fiducials were carefully removed and substituted with EPR-silent fiducials of identical diameter.

### III. RESULTS

Figure 2 presents the dependence of integral intensity of different projections as a function of the time over the image acquisition. For a sample with fixed spin probe concentration, the integral intensity of a projection does not depend on the gradient orientation and, therefore, is constant throughout the imaging time. In reality, the OX063 clearance from a tumor has an  $\sim 30$  min half-life time, which is comparable with the imaging time. Therefore, in the absence of continuous infusion, a decay of integral intensity of projections should be observed. Figure 2 shows that the concentration of spin label in the rabbit tumor gradually increased by approximately 15% during CW imaging and was stable for the ESE imaging time. From this, we conclude that the rate of continuous infusion during the imaging was at least sufficient if not slightly higher than necessary to compensate for the clearance.

Selected slices of CW and ESE concentration images are shown in Figs. 3(a) and 3(b). In the images  $Y$  axis denotes the axial direction from foot to thigh. The corresponding slices of anatomic MRI image registered to EPR images presented in Fig. 3(c). The  $T_2$  MRI image was segmented to include high  $T_2$  regions of the leg taken to correspond to tumor tissue, denoted by contours in EPR images. Note that while CW and ESE measurements exhibit similar concentra-

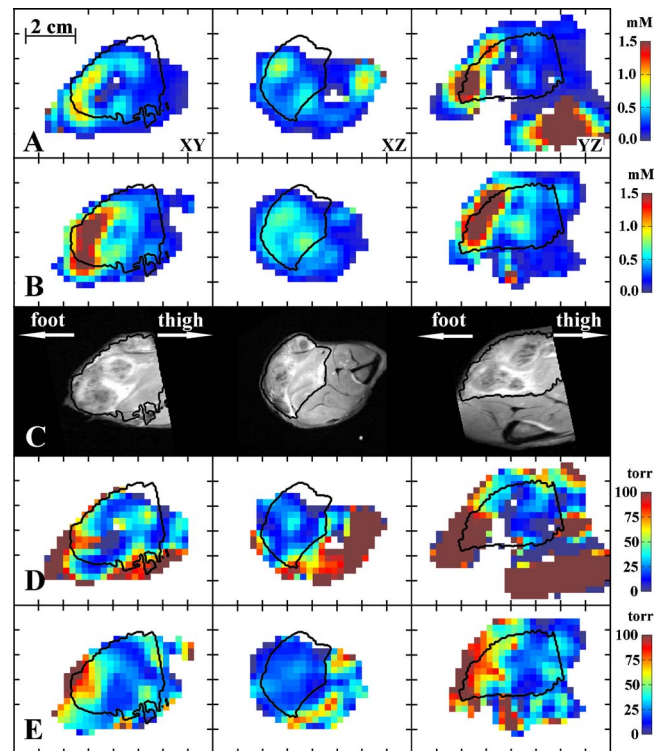


FIG. 3. Selected slices of images: (a) CW concentration, (b) ESE concentration, (c)  $T_2$  weighted MRI, (d) CW  $p\text{O}_2$ , and (e) ESE  $p\text{O}_2$ . The tumor region is determined from the MRI image and is outlined by contours.

tion pattern, the intensity of ESE is considerably higher: The mean concentration of spin probe in the tumor from the CW image is 0.53 mM and from the ESE image is 0.75 mM. Since the ESE image was obtained after the CW image, this confirms that the rate of the spin probe injection was higher than necessary. It is interesting to note that large amount of spin probe was accumulated in the portion of the tumor distant from the arterial infusion [see Figs. 3(a) and 3(b), toward foot] and the calf muscle adjacent to the knee [see Figs. 3(a) and 3(b), toward thigh]. The concentration of the spin probe in these areas reached 2–3 mM.

Figures 3(d) and 3(e) show slices of  $p\text{O}_2$  images corresponding to concentration image slices presented in Figs. 3(a) and 3(b). The image voxels within the tumor segment demonstrate much lower  $p\text{O}_2$  than within the muscle. Very high concentrations of spin probe that has been observed in the concentration images are shown to broaden spin packet spectral lines or decrease phase relaxation times  $T_2$ . The relaxation times in some areas of muscle became so short, that those areas became invisible to ESE images. The CW image faithfully reproduces the distribution of spin probe line width in these high concentration areas. However the concentration in excess of 1 mM induces line broadening that renders quantitative oxygen measurement problematic. On the other hand, most of the tumor received an amount of spin probe optimum for precise  $p\text{O}_2$  measurement. The histogram of the  $p\text{O}_2$  in the tumor is presented in Fig. 4. One can notice a broader distribution of  $p\text{O}_2$  in the CW image. The mean tumor  $p\text{O}_2$  determined from the CW image was 27 torr, while

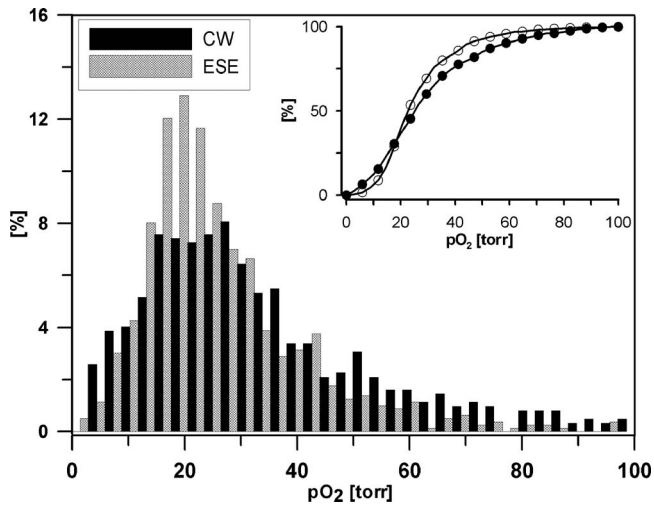


FIG. 4. The normalized frequency histogram of  $pO_2$  values in the tumor region determined using CW and ESE methodologies. The inset shows a cumulative histogram.

ESE measurements give 29 torr. The medians for CW and ESE  $pO_2$  images were both 24 torr. The hypoxic (below 10 torr) fractions for CW and ESE  $pO_2$  images were 0.22 and 0.04, respectively. For calculation of the means, medians, and hypoxic fractions, only the tumor regions with concentrations below 1 mM were used.

It is also interesting to note that in the tumor regions with hypoxia, the patterns of oxygenation are reproducible. Regions of higher and lower oxygenation can be seen from these randomly selected slices to be consistent within the image. The higher oxygenation regions are discordant, consistent with the difficulty of obtaining high oxygenation, high concentration region signal with ESE.

#### IV. DISCUSSION

It is of interest to compare the OX063 dose to that given to 20 g mice for tumor oxygen imaging.<sup>14</sup> For such mice, IV infusion of trityl involved a bolus of 50 mg, followed by continuous infusion of a similar amount per hour (1.2 g/kg b.w. for bolus and 1.4 g/kg b.w./h continuous infusion). A similar protocol was published elsewhere.<sup>19</sup> For the rabbit, this scales to 6 g of OX063 for the initial bolus plus an additional 6 g infused per hour following the bolus. Over 12 g of trityl would be used for the sequence of images obtained in this study. Intra-arterial administration of spin probe of 170 mg/kg b.w., one-seventh of the amount used for intravenous injection in mice produced signals in rabbit muscle factors of 3–5 higher than that in the muscle of mice. The signals observed in the rabbit tumor also exceed those found in mice tumors. Thus, a reduction in the amount of injected trityl per kg bodyweight by factors of 20–50 appears to be possible when delivered intra-arterially to selected anatomic regions such as an appendage. Although OX063 has been found to have minimal toxicity in animals, decreasing the amount of trityl per kg bodyweight not only decreases the cost of an experiment but will also reduce any potential spin probe toxicity in large animals.

A major problem associated with the imaging of large objects is the reduced  $B_1/\sqrt{W}$  efficiency of large resonators. Resonators with larger volumes require more power to generate magnetic field of the same magnitude and have lower sensitivity, inversely dependent on the volume of the resonator. Bulky animal tissues that have high losses further decrease the efficiency of a resonator by lowering the  $Q$ . The  $Q$  of the loaded resonator in this study was about 12. This is very low for CW acquisition, whose performance is dependent on  $Q$ . For ESE imaging, this  $Q$  is close to optimal<sup>27</sup> and, as a result, this methodology may be better suited for larger specimens. An additional concern associated with the increased resonator size is the fact that the size of 50 mm used in this study is close to 70 mm skin depth of RF field at 250 MHz in an approximate flat slab geometry.<sup>29</sup> These factors affect the quality and signal-to-noise ratio of images. Therefore, one should expect some technological limit for application of large size resonators. On the other hand, high resolution MRIs have been obtained using large resonators at frequencies substantially higher than this frequency, 325 MHz (Ref. 30) and 340 MHz.<sup>31</sup> The presented EPROI images and aforementioned MRI studies allowed us to anticipate that resonators with even larger volume may be used for EPR measurements.

The reduction in signal from the unit sample volume in large resonators can be compensated by either increasing measurement time or by sacrificing image resolution. We have used the latter. The estimation of the best spatial resolution of EPR image is given by ratio of the applied magnetic field gradient and spin probe line width. For the gradients used in this work this gives about 2 mm for CW measurements and 3 mm for pulse measurements. Taking into account that the image resolution cannot be better than twice the linear dimension of an image voxel size,<sup>21</sup> the final resolution of both modalities is close to 4 mm. This resolution is worse than the 1.4 mm resolution achieved for mouse tumor imaging.<sup>27</sup> While for CW imaging the major limiting factor is a signal-to-noise ratio per unit volume, ESE suffers from another limitation. ESE image projections are acquired in frequency space. The frequency content of a projection is proportional to the applied magnetic field gradient and the dimensions of the object. For correct reconstruction, the full frequency range of the object should be obtained. Instrumental bandwidth limitations force a restriction on maximum gradient strength and, as a result, lead to lower spatial resolution. Recent developments in our laboratory will eliminate this limitation.<sup>32</sup>

In general, EPR methodologies used in this study reveal the same information. Nevertheless, the CW and EPR images exhibit certain differences. Accumulation of the spin probe in some areas of the tumor led to trityl concentrations above 1 mM. At such concentrations, the EPR line of trityl in animals has been reported to have substantial broadening due to spin-spin interaction.<sup>19</sup> The CW image was able to reproduce these areas, while the ESE performance in these areas was found to be rather poor. Thus, for areas with high spin probe and  $pO_2$  concentration ESE may emphasize the low concen-

tration and  $pO_2$ . However, the main target of present tumor research focuses on low  $pO_2$  regions, areas of hypoxia in tumors. Also we are developing the means for more precise control of the administered spin probe dose which will prevent accumulation of very high spin probe concentrations in tissues. It should be noted that the ESE methodology allowed approximately four times shorter image acquisition time compared to that of CW. Phantom studies demonstrate an increase in  $pO_2$  resolution using the ESE technique relative to CW by factors of 2–3, making 1 torr resolution possible.<sup>27</sup> This may explain broader distribution of  $pO_2$  values as determined by the CW methodology.

## V. CONCLUSIONS

The injection of the spin probe directly into the artery feeding a rabbit leg bearing a VX-2 tumor allowed us to reduce, by nearly one order of magnitude, the amount of spin probe used and provided nearly five times more signal than has been found adequate for smaller animal imaging. Both CW and ESE imaging methodologies demonstrated good performance and produced high quality consistent  $pO_2$  images. This study paves the way for application of EPR imaging to the study of animals larger than mice and rats.

## ACKNOWLEDGMENTS

The authors acknowledge veterinary technicians at the Large Animals Clinical Services facility in University of Chicago, Jennifer McGrath and Karin Peterson for preparing the animal, and their colleague from the Center for EPR imaging *in vivo* physiology in University of Chicago, Dr. Colin Mailer for useful discussions and help in preparation of this manuscript.

This work was supported by NIH, Grant Nos. P41 EB002034 and R01 CA98575.

<sup>a)</sup> Author to whom correspondence should be addressed. Electronic mail: h-halpern@uchicago.edu

<sup>1</sup> L. J. Berliner and H. Fujii, "Magnetic-resonance imaging of biological specimens by electron-paramagnetic resonance of nitroxide spin labels," *Science* **227**, 517–519 (1985).

<sup>2</sup> H. J. Halpern, D. P. Spencer, J. Vanpolen, M. K. Bowman, A. C. Nelson, E. M. Dowey, and B. A. Teicher, "Imaging radio-frequency electron-spin-resonance spectrometer with high-resolution and sensitivity for *in vivo* measurements," *Rev. Sci. Instrum.* **60**, 1040–1050 (1989).

<sup>3</sup> H. J. Halpern, C. Yu, M. Peric, E. Barth, D. J. Grdina, and B. A. Teicher, "Oxymetry deep in tissues with low-frequency electron-paramagnetic-resonance," *Proc. Natl. Acad. Sci. U.S.A.* **91**, 13047–13051 (1994).

<sup>4</sup> P. Kuppusamy, M. Chzhan, K. Vij, M. Shteynbuk, D. J. Lefer, E. Giannela, and J. L. Zweier, "3-dimensional spectral spatial EPR imaging of free-radicals in the heart: A technique for imaging tissue metabolism and oxygenation," *Proc. Natl. Acad. Sci. U.S.A.* **91**, 3388–3392 (1994).

<sup>5</sup> B. Gallez, C. Baudelet, and B. F. Jordan, "Assessment of tumor oxygenation by electron paramagnetic resonance: Principles and applications," *NMR Biomed.* **17**, 240–262 (2004).

<sup>6</sup> H. J. Halpern, in *In Vivo EPR (ESR): Theory and Applications*, edited by L. J. Berliner (Kluwer Academic, New York/Plenum, New York, 2003), Vol. 18, pp. 469–482.

<sup>7</sup> B. B. Williams and H. J. Halpern, "In vivo EPR imaging," in *Biomedical EPR—Part A: Free Radicals, Metals, Medicine, and Physiology*, edited by S. S. Eaton, G. R. Eaton, and L. J. Berliner (Kluwer Academic, New York/Plenum, New York, 2005), Vol. 23, pp. 283–320.

<sup>8</sup> J. H. Ardenkjær-Larsen, I. Laursen, I. Leunbach, G. Ehnholm, L. G. Wistrand, J. S. Petersson, and K. Golman, "EPR and DNP properties of certain

novel single electron contrast agents intended for oximetric imaging," *J. Magn. Reson.* **133**, 1–12 (1998).

<sup>9</sup> J. S. Lewis, D. W. McCarthy, T. J. McCarthy, Y. Fujibayashi, and M. J. Welch, "Evaluation of  $^{64}Cu$ -ATSM *in vitro* and *in vivo* in a hypoxic tumor model," *J. Nucl. Med.* **40**, 177–183 (1999).

<sup>10</sup> W. J. Koh, J. S. Rasey, M. L. Evans, J. R. Grierson, T. K. Lewellen, M. M. Graham, K. A. Krohn, and T. W. Griffin, "Imaging of hypoxia in human tumors with [F-18] fluoromisonidazole," *Int. J. Radiat. Oncol., Biol., Phys.* **22**, 199–212 (1992).

<sup>11</sup> K. Golman, J. S. Petersson, J. H. Ardenkjær-Larsen, I. Leunbach, L. G. Wistrand, G. Ehnholm, and K. C. Liu, "Dynamic *in vivo* oxymetry using Overhauser enhanced MR imaging," *J. Magn. Reson. Imaging* **12**, 929–938 (2000).

<sup>12</sup> C. Baudelet and B. Gallez, "How does blood oxygen level-dependent (BOLD) contrast correlate with oxygen partial pressure ( $pO_2$ ) inside tumors?," *Magn. Reson. Med.* **48**, 980–986 (2002).

<sup>13</sup> D. S. Vikram, J. L. Zweier, and P. Kuppusamy, "Methods for noninvasive imaging of tissue hypoxia," *Antioxid. Redox Signal.* **9**, 1745–1756 (2007).

<sup>14</sup> M. Elas, B. B. Williams, A. Parasca, C. Mailer, C. A. Pelizzari, M. A. Lewis, J. N. River, G. S. Karczmar, E. D. Barth, and H. J. Halpern, "Quantitative tumor oxymetric images from 4D electron paramagnetic resonance imaging (EPRI): Methodology and comparison with blood oxygen level-dependent (BOLD) MRI," *Magn. Reson. Med.* **49**, 682–691 (2003).

<sup>15</sup> M. Elas, K. H. Ahn, A. Parasca, E. D. Barth, D. Lee, C. Haney, and H. J. Halpern, "Electron paramagnetic resonance oxygen images correlate spatially and quantitatively with oxylite oxygen measurements," *Clin. Cancer Res.* **12**, 4209–4217 (2006).

<sup>16</sup> C. R. Haney, A. D. Parasca, X. B. Fan, R. M. Bell, M. A. Zamora, G. S. Karczmar, H. J. Mauceri, H. J. Halpern, R. R. Weichselbaum, and C. A. Pelizzari, "Characterization of response to radiation mediated gene therapy by means of multimodality imaging," *Magn. Reson. Med.* **62**, 348–356 (2009).

<sup>17</sup> M. Elas, R. Bell, D. Hleihel, E. D. Barth, C. Mcfaul, C. R. Haney, J. Bielanska, K. Pustelny, K. H. Ahn, C. A. Pelizzari, M. Kocherginsky, and H. J. Halpern, "Electron paramagnetic resonance oxygen image hypoxic fraction plus radiation dose strongly correlates with tumor cure in FSA fibrosarcomas," *Int. J. Radiat. Oncol., Biol., Phys.* **71**, 542–549 (2008).

<sup>18</sup> C. C. Ling, J. Humm, S. Larson, H. Amols, Z. Fuks, S. Leibel, and J. A. Koutcher, "Towards multidimensional radiotherapy (MD-CRT): Biological imaging and biological conformality," *Int. J. Radiat. Oncol., Biol., Phys.* **47**, 551–560 (2000).

<sup>19</sup> K. Matsumoto, S. English, J. Yoo, K. Yamada, N. Devasahayam, J. A. Cook, J. B. Mitchell, S. Subramanian, and M. C. Krishna, "Pharmacokinetics of a triaryl-methyl-type paramagnetic spin probe used in EPR oximetry," *Magn. Reson. Med.* **52**, 885–892 (2004).

<sup>20</sup> B. B. Williams, H. al Hallaq, G. V. R. Chandramouli, E. D. Barth, J. N. Rivers, M. Lewis, V. E. Galtsev, G. S. Karczmar, and H. J. Halpern, "Imaging spin probe distribution in the tumor of a living mouse with 250 MHz EPR: Correlation with BOLD MRI," *Magn. Reson. Med.* **47**, 634–638 (2002).

<sup>21</sup> K. H. Ahn, V. S. Subramanian, and H. J. Halpern, "Scaling of EPR spectral-spatial images with size of sample: Images of a sample greater than 5 cm in linear dimension," *Med. Phys.* **34**, 4854–4859 (2007).

<sup>22</sup> C. R. Haney, X. Fan, A. D. Parasca, G. S. Karczmar, H. J. Halpern, and C. A. Pelizzari, "Immobilization using dental material casts facilitates accurate serial and multimodality small animal imaging," *Concepts Magn. Reson., Part B* **33B**, 138–144 (2008).

<sup>23</sup> K. H. Ahn and H. J. Halpern, "Spatially uniform sampling in 4-D EPR spectral-spatial imaging," *J. Magn. Reson.* **185**, 152–158 (2007).

<sup>24</sup> K. H. Ahn and H. J. Halpern, "Simulation of 4D spectral-spatial EPR images," *J. Magn. Reson.* **187**, 1–9 (2007).

<sup>25</sup> K. H. Ahn and H. J. Halpern, "Object dependent sweep width reduction with spectral-spatial EPR imaging," *J. Magn. Reson.* **186**, 105–111 (2007).

<sup>26</sup> C. Mailer, B. H. Robinson, B. B. Williams, and H. J. Halpern, "Spectral fitting: The extraction of crucial information from a spectrum and a spectral image," *Magn. Reson. Med.* **49**, 1175–1180 (2003).

<sup>27</sup> B. Epel, S. V. Sundramoorthy, C. Mailer, and H. J. Halpern, "A versatile high speed 250-MHz pulse imager for biomedical applications," *Concepts Magn. Reson., Part B* **33B**, 163–176 (2008).

<sup>28</sup> S. V. Sundramoorthy, B. Epel, C. Mailer, and H. J. Halpern, "A passive

- dual-circulator based transmit/receive switch for use with reflection resonators in pulse electron paramagnetic resonance,” *Concepts Magn. Reson., Part B* **35B**, 133–138 (2009).
- <sup>29</sup>P. Röschmann, “Radiofrequency penetration and absorption in the human body: Limitations to high-field whole-body nuclear-magnetic-resonance imaging,” *Med. Phys.* **14**, 922–931 (1987).
- <sup>30</sup>R. E. Burgess, Y. Yu, A. M. Abduljalil, A. Kangarlu, and P. M. L. Robitaille, “High signal-to-noise flash imaging at 8 Tesla,” *Magn. Reson. Imaging* **17**, 1099–1103 (1999).
- <sup>31</sup>P. M. L. Robitaille, A. Kangarlu, and A. M. Abduljalil, “RF penetration in ultra high field MRI: Challenges in visualizing details within the center of the human brain,” *J. Comput. Assist. Tomogr.* **23**, 845–849 (1999).
- <sup>32</sup>S. Seifi, B. Epel, S. Subramanian, J. Bryant, C. Mailer, and H. J. Halpern, presented at the 51st Rocky Mountain Conference on Analytical Chemistry, EPR Symposium, Snowmass, CO, 2009 (unpublished).
- <sup>33</sup>C. Mailer, S. V. Sundramoorthy, C. A. Pelizzari, and H. J. Halpern, “Spin echo spectroscopic electron paramagnetic resonance imaging,” *Magn. Reson. Imaging* **55**, 904–912 (2006).